Accepted Manuscript

A smartphone-based point-of-care quantitative urinalysis device for chronic kidney disease patients

Shaymaa Akraa, Tran Tam Anh Pham, Haifeng Shen, Youhong Tang, Ben Zhong Tang, Jimmy Li, Sandy Walker

PII: S1084-8045(18)30144-9

DOI: 10.1016/j.jnca.2018.04.012

Reference: YJNCA 2126

To appear in: *Journal of Network and Computer Applications*

Received Date: 13 December 2017

Revised Date: 16 March 2018

Accepted Date: 23 April 2018

Please cite this article as: Akraa, S., Anh Pham, T.T., Shen, H., Tang, Y., Tang, B.Z., Li, J., Walker, S., A smartphone-based point-of-care quantitative urinalysis device for chronic kidney disease patients, *Journal of Network and Computer Applications* (2018), doi: 10.1016/j.jnca.2018.04.012.

A Smartphone-based Point-of-Care Quantitative Urinalysis Device for Chronic Kidney Disease Patients

Shaymaa Akraa[a], Tran Tam Anh Pham[a], Haifeng Shen[a,*], Youhong Tang[a,*], Ben Zhong Tang[b], Jimmy Li[a], Sandy Walker[a]

[a] *College of Science and Engineering, Flinders University, Adelaide, Australia*
[b] *Department of Chemistry, Division of Biomedical Engineering, The Hong Kong University of Science & Technology, China*

Abstract

This paper presents the design and development of a smartphone-based urinalysis device that has the ability for chronic kidney disease (CKD) patients themselves to conduct rapid and reliable quantitative urinalysis of human serum albumin (HSA) using an aggregation-induced emission (AIE) nanomaterial bioprobe with their own smartphones. The focus of this paper is a novel solution to the device agnosticism issue as a wide diversity of smartphones co-exist in the market. The solution comprises: a) custom-design and fabrication of an imaging housing that provides a consistent imaging condition regardless of the physical dimensions and the camera position of the smartphone used, b) orchestration of an image processing and analysis process that produces consistent image colour intensity values regardless of the camera sensor and imaging software used by the smartphone, and c) special design and development of an intuitive cross-platform mobile application that is scalable to growth, adaptable to changes, resilient to loss of data, and has an extremely low requirement for smartphone hardware. Preliminary evaluation of the device has confirmed the effectiveness of the proposed solution and the viability of such a smartphone-based device for people who have already developed or are prone to CKD to regularly perform point-of-care (POC) urine testing in order to self monitor their own health conditions without the burden of frequent visits to their doctors.

Keywords: chronic kidney disease, urinalysis, microalbuminuria, smartphone, device agnosticism, point-of-care

1. Introduction

The kidney is one of the most vital organs in the human body, with its primary function of filtering the blood to remove wastes and toxins. In addition, the kidney is responsible for regulating blood pressure, water balance in the body and vitamin D activation. Chronic kidney disease (CKD) is a major health issue worldwide. More than 500 million people - 7% of the world's population - have some form of CKD, causing millions of deaths every year [1]. In Australia alone, over 1/3 of the population aged over 65 is at risk of CKD and yet many of them are unaware of that [2]. Early and regular testing of high-risk groups - such as people with diabetes, hypertension, cardiovascular disease, and family history of kidney failure - can prevent from progressing to end-stage kidney disease (ESKD) that may result in dialysis, transplantation, and renal replacement therapy outcomes [3, 4]. In Australia, age-standardised incidence of ESKD is significantly higher in Aboriginal and Torres Strait Islander people compared with other Australians mainly due to limited access to early detection facilities [5], which if available, treatment with medication, dietary and appropriate changes to their lifestyle would be more effective [6].

Urinalysis - urine diagnosis - is a standard method for the identification of people at earlier time points in the trajectory of CKD when it does not necessarily produce signs or symptoms. One urinalysis method is to measure the amount of Human Serum Albumin (HSA) [7], a serum protein that would normally be present at high concentration levels in blood and should not appear in urine more than a clinically normal threshold value of 30 mg/dL. Early stage of kidney damage would allow a small amount of albumin to leak into urine, leading to the condition of microalbuminuria that exhibits albumin levels of more than 30 mg/dL in urine [8, 9]. Microalbuminuria urinalysis measures albumin concentration levels in various urine specimens, every few hours within a 24-hour window in order to produce a reliable result [10]. It relies on bulky and costly bench-top urine analysers and trained skills only available in laboratory settings, thereby requiring successive patient visits to clinics or hospitals and long turnaround times [11].

Point-of-care (POC) testing is preferred to laboratory urinalysis as it can provide rapid results on the site, partic-

*Corresponding authors. Tel.: +61 8 8201 3969 (Haifeng Shen), +61 8 8201 2138 (Youhong Tang).

Email addresses: akra0002@flinders.edu.au (Shaymaa Akraa), pham0172@flinders.edu.au (Tran Tam Anh Pham), haifeng.shen@flinders.edu.au (Haifeng Shen), youhong.tang@finders.edu.au (Youhong Tang), tangbenz@ust.hk (Ben Zhong Tang), jimmy.li@finders.edu.au (Jimmy Li), sandy.walker@finders.edu.au (Sandy Walker)

ularly suitable for screen for prevention, treatment monitoring, and patient self-testing [12, 13, 14]. A common urine testing method is colorimetric investigation utilising dipstick - a narrow plastic strip equipped with different sensitive chemical components. This method relies on the colour change of the chemical components, after their interaction with urine. There are many types of devices based on this method in the market, such as those from Dirui, Cormay, Spinreact, Roche, Siemens, Rayto, PocketChem and Arkray. Common to these devices is that they are limited by the time sensitivity of the chemical components and can only provide qualitative results due to their low sensitivity to albumin at 150 mg/dL [15, 16, 17]. More recently launched reagent strip devices such as Siemens DCA Vantage Analyzer [18] are capable of producing semi-quantitative results, however they are designed for doctors to use in clinics as they are still costly and not portable enough to be a viable solution for POC self-urinalysis.

While smartphones are widespread and becoming increasingly sophisticated, they have promoted remote diagnosis and telemedicine by building smartphone accessories and applications [19, 20]. For instance, mobile images can be used in pathology [21, 22, 23] to assist monitoring changes over time for some diseases, such as cardiology [24], blood cholesterol [25], glucose [26], pH [27], dermatology [28], neurosurgery [29, 30], microscopy [31], and ophthalmology [32]. These devices generally have a stringent requirement on the image quality especially intensity of colours as a slight drift would lead to inaccurate quantification [31]. However smartphones are notorious for their wide diversity of which a multiplicity of camera sensors and image software present a major hurdle to these applications as different phones would produce images of different quality even under exactly the same imaging condition. Therefore, device agnosticism is a paramount issue in these types of medical devices.

Smartphone-based urinalysis applications are also on the rise and the vast majority use smartphones as an alternative colorimetric analyser of urine dipsticks [33, 34, 35, 36, 37, 38] as they can provide spectrometric functions comparable to those offered by specialised urine dipstick readers at a much lower cost. However, these applications also share the same shortcomings inherited from the dipstick method: (a) the diagnosis is largely qualitative or at most semi-quantitative, depending on the types of reagent strips used, and (b) the diagnosis has a limited low range of albumin detection higher than the threshold of CKD due to the low sensitivity of the chemical components in the reagent strip. In addition, most of these applications do not use an imaging blackbox, making a test highly subject to the ambient light condition as well as the distance/alignment between the dipstick and the camera. Moreover, none of these applications has attempted to address the device agnosticism issue probably because the impact of image quality on a qualitative or semi-quantitative test result is not significant.

An alternative solution to smartphone-based urinalysis is to image and automatically analyse assays confined within disposable test tubes for full-quantitive detection of albumin in urine, which is only available through laboratory pathology. Our proposed urinalysis device - uTester - falls into this category, while the only other work that is publicly known is Albumin Tester [11], which uses a custom-built imaging housing for guaranteeing stable imaging conditions, a fluorescence-based detection kit for achieving full-quantitative urinalysis, and a specially designed smartphone application for visualising testing process and result.

The major differences between uTester and Albumin Tester are as follows. First, uTester explores a new test reagent BSPOTPE that is based on aggregation-induced emission (AIE) nanomaterial bioprobes [39], whereas Albumin Tester uses a commercial reagent - Albumin blue 580 - from Active Motif [40]. While Albumin Tester requires two test tubes filled with different reagents for the purpose of calibration, uTester only requires one test tube filled with the AIE reagent. Second, Albumin Tester measures the fluorescent signals of both tubes and models a linear relationship between the Relative Fluorescence Unit (RFU) value and the albumin concentration, whereas uTester uses image processing and analysis to model a linear relationship between the luminance of the imaged tube and the albumin concentration. Last but not least, Albumin Tester requires a special external lens and an optical filter in order to accurately detect fluorescent signals, whereas uTester only requires an optical filter to work with the smartphone's built-in lens. All in all, the most significant improvement in our work is a novel solution to the device agnosticism issue, which was not addressed in Albumin Tester.

In this paper, we present the design and development of the uTester urinalysis device that has the ability for CKD patients themselves to conduct rapid and reliable quantitative diagnosis of albumin in urine using their own smartphones. While our prior work bas proved the feasibility of such a device [41], this paper is focussed on a solution to device agnosticism. The solution comprises: a) custom-design and fabrication of an imaging housing that provides a consistent imaging condition regardless of the physical dimensions and the camera position of the smartphone used, b) orchestration of an image processing and analysis process that produces consistent image colour intensity values regardless of the camera sensor and image software used by the smartphone, and c) special design and development of an intuitive cross-platform mobile application that is scalable to growth, adaptable to changes, resilient to loss of data, and has an extremely low requirement for smartphone hardware.

The device consists of five key components: the smartphone, the albumin test reagent BSPOTPE, the imaging housing, the image processing and analysis techniques underpinning the mobile application, and mobile application itself. The rest of the paper is organised in that order. Section 2 introduces BSPOTPE, followed by the design of

the imaging housing in Section 3. After that, Section 4 presents the image processing and analysis process techniques, followed by the architecture of the mobile application in Section 5. Finally Section 6 concludes the paper with a summary of major contributions and future work.

2. BSPOTPE: A Novel Bioprobe for Albumin Detection and Quantification

Researchers are in enthusiastic pursuit of fluorescent bioprobes as they allow direct visualisation of bioanalytes on site and in time, and offer useful insights into complex biological structures and processes. Light emissions from conventional fluorophores are often quenched at high concentrations or in aggregate state, known as aggregation caused quenching (ACQ). Aggregation induced emission (AIE) refers to the observed phenomenon that a group of fluorogenic molecules that are non-emissive when molecularly dissolved but highly emissive when aggregated. The restriction of intramolecular rotations (RIR) is proposed as its main cause [42].

BSPOTPE is an environmentally stable and synthetically readily accessible FL (Fluorescent Light) probe for albumin detection and quantification [39]. It is unperturbed by the miscellaneous bioelectrolytes in the artificial urine. The non-luminescent BSPOTPE becomes emissive in the present of albumin. A set of experiments were conducted to understand how BSPOTPE responds to (in terms of FL intensity) albumin concentration in Artificial Urine (AU), which was prepared following Chutipongtanate's AU-Siriraj protocol [43], with pH of 6.8 and gravity of 1.010 g/ml. PBS (Phosphate-buffered saline) was made according to the cold spring harbor laboratory protocol [44]. All experiments were performed at room temperature. Steady-state fluorescence spectra were recorded on a Varian Cary Eclipse Fluorimeter, with excitation wavelength 340 nm and emission spectrum of 400-600 nm. Stock solution of BSPOTPE of a concentration of 5.0mM was prepared by dissolving an appropriate amount of dye in Milli-Q lab water. The solution was stored in dark room before use. Stock solutions of BSA (Bovine Serum Albumin) and HSA with a concentration of 8.0 mM were prepared by dissolving appropriate amounts of the protein in the PBS buffer. The solution was stored in aliquots at $-20°C$.

The final concentration of BSA and HSA in PBS was double checked by measuring its absorbance at 279 nm. Before preforming each experiment, the BSA concentration in AU was monitored according to protein dipstick grading. Three different concentrations of BSA, 1+ of 30 mg/dL, 2+ of 100 mg/dL and 3+ of 300 mg/dL [45], were incubated with different concentrations of BSPOTPE (0-50 μM) for 2 minutes, and the FL values were subsequently measured on the fluorimeter, as shown in Figure 1(a), (b) and (c) respectively. It is clear from Figure 1 that the FL threshold value for this type of fluorimeter is 1000 a.u. Higher than that, the equipment is unable to measure it.

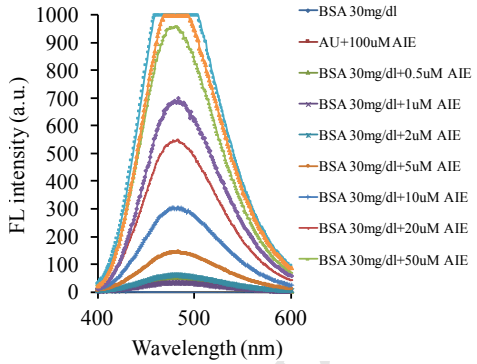

(a) AU with 30 mg/dL BSA

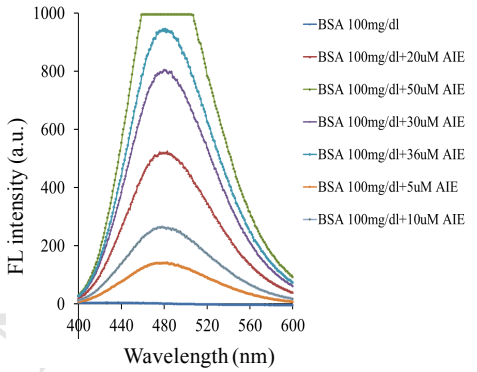

(b) AU with 100 mg/dL BSA

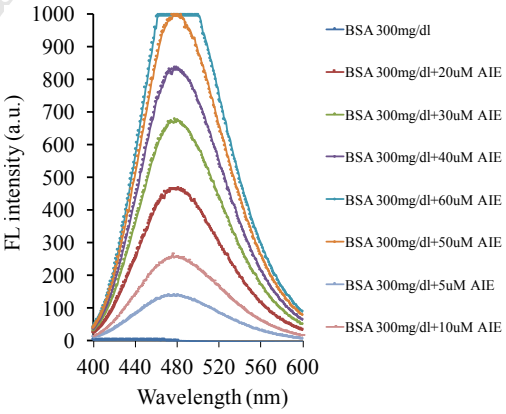

(c) AU with 300 mg/dL BSA

Figure 1: FL intensity of different BSPOTPE concentrations in AU with different BSA concentrations

According to Figure 2, the best working concentration of BSPOTPE monitoring BSA was optimised to be 30 μM. Higher concentration of BSPOTPE will cause the FL intensity value to exceed the threshold of 1000 a.u. as previously stated. Different concentrations of HSA in the range of 0-3000 ng/mL (0-300 mg/dL) were incubated with 30 μM BSPOTPE for 2 minutes, and the FL values were subsequently measured by the fluorimeter, as shown in Figure 3. Figure 4 shows the result from the experiments that the FL intensity measured by the fluorimeter responds linearly to the HSA concentration in the range of 0-400 ng/mL (0-40 mg/dL) in the AU specimen with 30

μM BSPOTPE, which confirms earlier findings [46, 47]. This result indicates that the fluorimeter-based solution can be used for urinalysis of up to 1+ microalbuminuria. However, albumin quantification based on FL intensity is not a practical solution to POC urinalysis as FL intensity has to be measured by a fluorimeter, such as a Varian Cary Eclipse Fluorimeter used in the experiments, which is expensive and not portable at all.

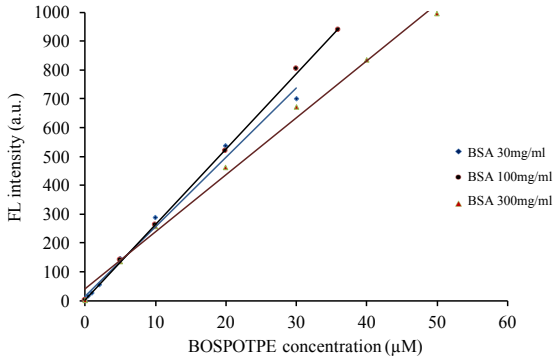

Figure 2: The best working concentration of BSPOTPE

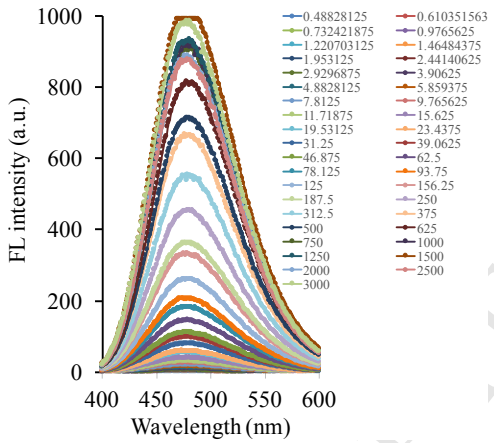

Figure 3: FL intensity of different HSA concentrations (ng/mL) in AU with 30μM BSPOTPE

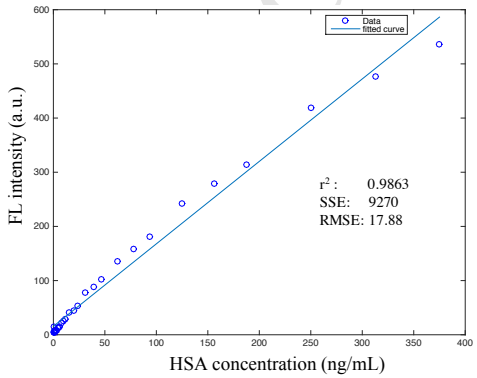

Figure 4: Linear correlation between FL intensity and HSA concentration in the range of 0-400 ng/mL

3. Imaging Housing and Camera Calibration

To use BSPOTPE in a smartphone-based urinalysis device, we propose an alternative solution to measuring FL intensity by first capturing the image of the fluorescent emission emerging from the test tube using the smartphone camera, then processing the image and analysing its properties, and finally representing the FL intensity with the image's colour luminance property that defines the amount of emitted light [48].

In order to create a consistent imaging condition, we have custom-designed and fabricated an imaging housing using Direct Digital Manufacture technique. It is able to support a wide range of smartphones with different dimensions and camera positions. Design of the housing was guided by the following requirements.

- *Using affordable and accessible manufacturing technologies:* the device must be usable and marketable to people with diverse abilities, and can be manufactured locally using technologically appropriate fabrication such as Laser Cutting and/or 3D Printing.
- *User-friendly:* the device should be easy to use by elderly users without prior experience or training. Age-related cognitive decline is related to slower and less intuitive performance with contemporary devices and interfaces, resulting from a lack of familiarity and capability. Intuitive interaction therefore involves the use of knowledge gained from other products and/or experiences [49, 50]. Therefore, devices that people use intuitively are those with features, functions and/or processes that they have encountered before.
- *Effective, efficient, and satisfactory:* a user-centric self-diagnostic device has little value, unless it can be easily accessed and used by the product's target user. To this end, the device must be effective (the extent to which a certain goal is achieved), efficient (where the amount of effort and cost required, is commensurate to the value of the goal achieved) and provide satisfaction (within a specified context and user type).
- *Adaptable to camera postion:* the device caters for smartphones with different camera positions, such as in the top-middle or top-left corner.
- *Blocking external light:* a blackbox design to prevent external light contamination.

As shown in Figure 5(a), the external housing is a proof-of-concept optomechanical blackbox installed on the existing camera unit of the smartphone for holding the test tubes and for blocking external light. Further illustrated by Figure 5(b), the imaging housing contains two tube holders and two battery-operated LED lighting sources with specific optical filters: one tube filled with the BSPOTPE reagent triggered by a UV lighting source for testing albumin concentration and the other tube holder

and lighting source reserved for testing creatinine in the future in order to measure albumin-to-creatinine ratio (ACR), the clinical standard. Controls are provided to align one of two tube holders together with its lighting source and optical filter right with the smartphone's camera in order to provide a stable and consistent condition for capturing images from reagent assays.

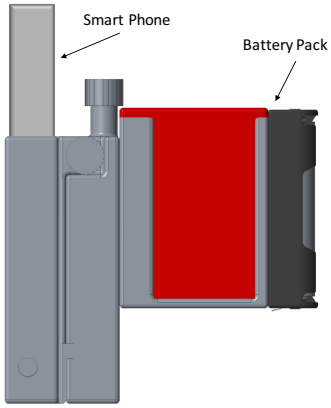

(a) Exterior design

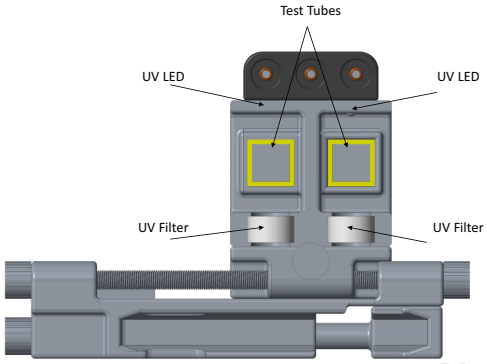

(b) Interior design

Figure 5: Imaging housing attached to a smartphone

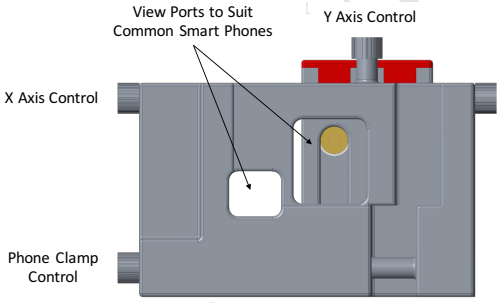

Figure 6: Adjustable viewports and clamp controls

To support a variety of smartphones in the market, the imaging housing is lightweight and adjustable to work with existing smartphones that have different dimensions and camera positions through adjustable viewports and clamp controls, as shown by Figure 6.

To further ensure a consistent imaging condition across different smartphones, we calibrate their cameras by setting the same configuration as follows:

- Setting the image size of 3264x2448 (4:3) (8M).
- Choosing a low ISO of 200/100 to avoid noise in order to capture a high quality image under low light conditions [51]. ISO controls the sensitivity of a camera's sensor.
- Set Auto White Balance (AWB) into Daylight to preserve the colour response as a constant [52, 53]. AWB algorithms try to account for changes in human visual sensitivity under different ambient illuminant conditions [54].
- Turning off High Dynamic Range (HDR). HDR is used to increase the span between shadows and highlights in an image [55].

4. Image Processing and Analysis

After obtaining the images from a smartphone equipped with the housing, we need to decide which method should be used to transform the visible electromagnetic spectrum (colour) into a digital signal. In other words, we need to choose the best model to represent the colour intensity that well responds to the FL intensity. The human visual system often perceives colours by brightness attributes while a computer can describe a colour by using the RGB (Red, Green, Blue) model [56]. However RGB is not the best way to represent images in the real world as it is psychologically non-intuitive and perceptually non-uniform [57]. We therefore choose the HSL (Hue, Saturation, Lightness) model as it is cognitive and intuitive for humans. It is broken down according to physiological criteria: hue refers to the pure spectrum colour and corresponds to the prevailing colour as perceived by a human, saturation refers to the proportional purity, and luminance refers to the amount of light in a colour [58]. We are especially interested in the luminance (i.e. intensity) of a particular colour in the captured image as it corresponds to the FL intensity we need to measure. The process of transforming an image to retrieve a colour luminance value is described as follows.

1. Identify a region of 32×32 with uniform and homogeneous colour within the centre of the image.
2. Transform the RGB colour space of the selected region into the HSL colour space.
3. Calculate the mean values of the intensity band of the HSL colour space from the selected region.
4. Retrieve the mean lightness value from the HSL colour space to represent the luminance colour band of the region.

However, before we can retrieve the luminance values of images taken by different phones, it is worth noting that image colours captured by one camera are likely different from those by another camera for the same scene. This problem even occurs for the same type of smartphones [59]. Therefore, cameras of both different and same models cannot exhibit substantially consistent colour responses and the differences can lead to considerable errors in scene interpretation [60]. This issue is essentially

related to the diversity of camera sensors used by different phones to capture images as well as to the different gamma values used by smartphone software to compensate and correct the errors caused by the non-linear response of modern CMOS (complementary metal-oxide-semiconductor) image sensors [61].

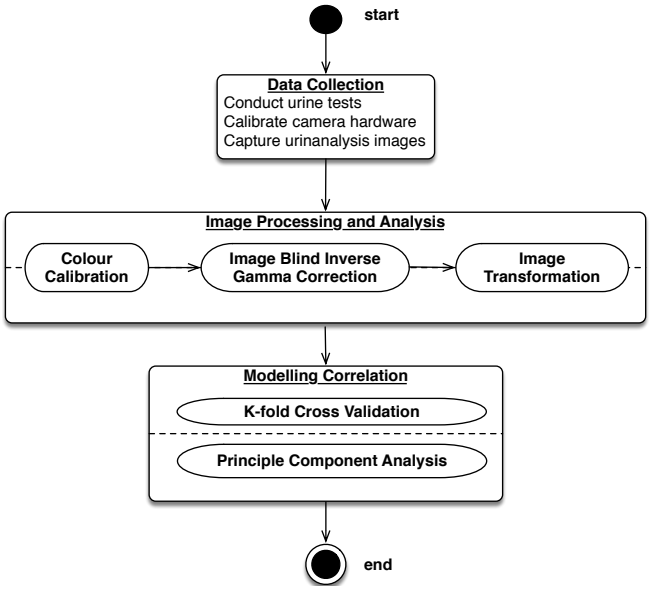

Figure 7: The imaging processing and analysis process

To address this issue, we propose an imaging processing and analysis process as illustrated in Figure 7, which starts with data collection by first calibrating camera hardware and then capturing urinalysis images from the urine tests. After capturing a sequence of urinalysis images corresponding to different albumin concentration levels, the process proceeds to image processing and analysis consisting of a series of sub-processes in the order of colour calibration, image blind inverse gamma correction, and image transformation. The final stage of the process is to model a relationship between image luminance values and HSA concentration levels through a modelling technique such as Principle Component Analysis (PCA) or K-fold cross-validation.

4.1. Colour Calibration

A more accurate improvement must be applied to images captured by the already calibrated cameras. However, the effect of software improvement must be kept to a minimum in order to avoid amplifying noise, clamping and colour space distortion errors. Three different post-processing methods are found useful to improve the results, including linear least squares matching, 3x3 RGB to RGB linear transform, and general polynomial transform. A 3x3 RGB to RGB linear transform is one of the common post-processing methods used to account for the inter-channel effects [60]. It transforms the 24 colour samples of a camera image into the parallel colour samples of a target image. The following matrix is the key solution to the over-constrained matrix system:

$$\begin{bmatrix} \overrightarrow{I_1} \\ \overrightarrow{I_2} \\ \cdots \\ \overrightarrow{I_{24}} \end{bmatrix}_{24\times 3} \times \begin{bmatrix} t_{rr} & t_{rg} & t_{rb} \\ t_{gr} & t_{gg} & t_{gb} \\ t_{br} & t_{bg} & t_{bb} \end{bmatrix}_{3\times 3} \simeq \begin{bmatrix} \overrightarrow{T_1} \\ \overrightarrow{T_2} \\ \cdots \\ \overrightarrow{T_{24}} \end{bmatrix}_{24\times 3},$$

which can be rewritten as a linear system below:

$$\begin{bmatrix} \overrightarrow{I_1} & \overrightarrow{O_3} & \overrightarrow{O_3} \\ \overrightarrow{O_3} & \overrightarrow{I_1} & \overrightarrow{O_3} \\ \overrightarrow{O_3} & \overrightarrow{O_3} & \overrightarrow{I_1} \\ \overrightarrow{I_2} & \overrightarrow{O_3} & \overrightarrow{O_3} \\ \overrightarrow{O_3} & \overrightarrow{I_2} & \overrightarrow{O_3} \\ \overrightarrow{O_3} & \overrightarrow{O_3} & \overrightarrow{I_2} \\ \cdots & \cdots & \cdots \\ \overrightarrow{I_{24}} & \overrightarrow{O_3} & \overrightarrow{O_3} \\ \overrightarrow{O_3} & \overrightarrow{I_{24}} & \overrightarrow{O_3} \\ \overrightarrow{O_3} & \overrightarrow{O_3} & \overrightarrow{I_{24}} \end{bmatrix}_{72\times 9} \times \begin{bmatrix} t_{rr} \\ t_{rg} \\ t_{rb} \\ t_{gr} \\ t_{gg} \\ t_{gb} \\ t_{br} \\ t_{bg} \\ t_{bb} \end{bmatrix}_{9} \simeq \begin{bmatrix} \overrightarrow{T_1^T} \\ \overrightarrow{T_2^T} \\ \cdots \\ \overrightarrow{T_{24}^T} \end{bmatrix}_{72}$$

$$\Leftrightarrow A \times \overrightarrow{t} \simeq \overrightarrow{T} \Leftrightarrow \simeq Pinv(A) \times \overrightarrow{T}. \quad (1)$$

The matrix elements are grouped into vectors as follows:

1. The first vector denotes the colour of camera image samples in the format of $\overrightarrow{I} = [I_r, I_g, I_b]$,
2. The second vector denotes the colour for target image sample in the format of $\overrightarrow{T_s} = [T_{rs}, T_{gs}, T_{bs}]$, and
3. The third vector denotes the 3-component null vector in the format of $\overrightarrow{O} = [0, 0, 0]$.

In addition, t_{xy} is the idiom that specifies how much the input from colour channel x contributes to the output of colour channel y. Singular value decomposition is used to compute the pseudo-inverse of matrix A and back substitution is used to compute the solution $\overrightarrow{t}$ [60].

Despite the fact that the RGB to RGB matrix transform calculates for inter-channel effects, it does not have a translation component and does not compensate for non-linearities in the response functions. To account for these remaining shortcomings, we devise a general polynomial transform, where the 3×3 RGB to RGB transform is generalised to a non-linear transform by introducing higher degree terms to recompense for the nonlinearities in the response functions and a bias term to allow for translations. The general formula for colour $c \in \{r, g, b\}$ of sample s is:

$$\sum_{k=1}^{D} (t_{rc_k} Ir_s^k + t_{gc_k} Ig_s^k + t_{bc_k} Ib_s^k) + t_{c0} \simeq T_{C_s},$$

where D is the degree of the polynomial approximation; Ir_s^k, Ig_s^k, and Ib_s^k are the red, green and blue values for camera image sample s, raised to power k respectively; T_{C_s} is the value for colour channel c of target image sample s; t_{xc_k} is the polynomial coefficient of the k^{th} order term that designates how much the input from colour channel

$x \in \{r, g, b\}$ subscribes to the output of colour channel c; and t_{c0} is an additional term that allows translating the output of channel c.

Our experiments have shown that $D = 2$ is sufficient to fulfil the level of accuracy required by our application. For $D = 2$, we can re-write Equation 1 for all the 24 samples of the colour chart in an equivalent matrix form as follows:

$$\begin{bmatrix} Ir_1 & Ir_1^2 & Ig_1 & Ig_1^2 & Ib_1 & Ib_1^2 & 1 \\ Ir_2 & Ir_2^2 & Ig_2 & Ig_2^2 & Ib_2 & Ib_2^2 & 1 \\ \cdots & \cdots & \cdots & \cdots & \cdots & \cdots & 1 \\ Ir_{24} & Ir_{24}^2 & Ig_{24} & Ig_{24}^2 & Ib_{24} & Ib_{24}^2 & 1 \end{bmatrix}_{24\times 7}$$

$$\times \begin{bmatrix} t_{rc_1} & t_{rc_2} & t_{gc_1} & t_{gc_2} & t_{bc_1} & t_{bc_2} & t_{r0} \end{bmatrix}_7^T \simeq \begin{bmatrix} T_{C_1} \\ T_{C_2} \\ \cdots \\ T_{C_{24}} \end{bmatrix}_{24}$$

$$\Leftrightarrow B \times \overrightarrow{t_c} \simeq \overrightarrow{T_c} \Leftrightarrow \overrightarrow{t_c} \simeq Pinv(B) \times \overrightarrow{T_c}, c \in \{r, g, b\}.$$

Each matrix equation is solved by using singular value decomposition in order to compute the pseudo-inverse of matrix B and back substitution to compute the 3 solutions $\overrightarrow{t_r}$, $\overrightarrow{t_g}$, and $\overrightarrow{t_b}$. It is worth mentioning that matrix B remains the same for all three-colour channels; therefore, there is a need to perform the inversion of matrix only once [60].

Algorithm 1 describes the image calibration process for one smartphone. Images captured by each smartphone needs to be individually calibrated.

Algorithm 1: $ImgCal(img\_rgb, img\_src)$: img_cal

Require: img_rgb: vector of standard RGB colour images captured by the smartphone
Require: img_src: vector of urinalysis images captured by the smartphone
Ensure: img_cal: vector of calibrated urinalysis images for the smartphone
1: $cal\_mat \leftarrow \overline{img\_rgb} \times std\_rgb$ {std_rgb: vector of standard RGB colours}
2: **for** $(\forall I_i \in img\_src)$ **do**
3: $\quad img\_cal[i] \leftarrow I_i \times cal\_mat$
4: **end for**
5:
6: **return** img_cal

4.2. Blind Inverse Gamma Correction

The value of γ is typically determined experimentally in the absence of any calibration information or knowledge of the imaging device, for example, downloading an image from the web. Moreover, most commercial digital cameras dynamically vary the amount of gamma. The blind inverse gamma correction technique is used to estimate the amount of gamma correction. The basic tactic exploits the fact that *gamma correction introduces specific higher-order correlations in the frequency domain. These correlations can be detected using tools from polyspectral analysis. The amount of gamma correction is then determined by minimising these correlations* [62]. The method assumes that gamma correction can be modeled with the one-parameter family of functions: where $g(u) = u^\gamma$ indicates the image pixel colour intensity. It is worth mentioning that rescaling intensity into a new range of [0, 1] does not affect the bicoherence. As only the gamma corrected images are available in our application, the main task is to determine the value of γ. To this end, we apply a range of inverse gamma values to each image and select the value that minimises the third-order correlations as in Equation 2.

$$\sum_{w1=-\pi}^{\pi} \sum_{w2=-\pi}^{\pi} |\hat{b}(w1, w2)|, \tag{2}$$

where $\hat{b}(w1, w2)$ is the bicoherence, which is defined in Equation 3:

$$\hat{b}(w1, w2) = \frac{|\frac{1}{N}\sum_k Y_k(w1)Y_k(w2)Y_k(w1+w2)|}{\sqrt{\frac{1}{N}\sum_k |Y_k(w1)Y_k(w2)|^2 \frac{1}{N}\sum_k |Y_k(w1+w2)|^2}}. \tag{3}$$

To avoid excessive demand of memory when computing an image's full four-dimensional bicoherence, our analysis is bounded to the one-dimensional horizontal scan lines of an image. One example to get the bicoherence for each 1-D image slice $y(n)$ is computed by dividing the signal, which has one dimension, into overlapping segments each of which has a length of 64 with an overlap of 32 pixels. A 128-point windowed DFT (Discrete Fourier transform) $Y_K(w)$ is estimated for each segment from which the bicoherence is estimated, that is $\hat{b}(w1, w2)$ as in Equation 3. Also, there should be a balance between the segment length and the number of segments. Empirically, the parameters have presented good compromise [62].

Algorithm 2 describes the blind inverse gamma correction process.

4.3. Modelling the Correlation

We first performed experiments using BSPOTPE bioprobe for urine specimens with albumin concentration levels in the range of 0-700 ng/mL (0-70 mg/dL) and captured the urinalysis images using three different smartphones: iPhone 6s (iP), Galaxy Note 4 (N4), and Galaxy S3 (S3). Figure 8 shows the urinalysis images captured by the 3 smartphones.

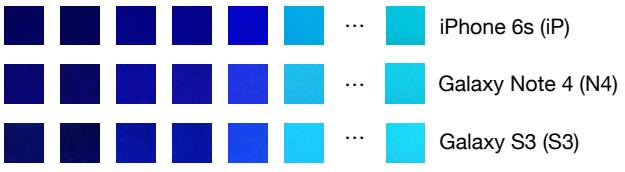

Figure 8: Images of different albumin concentration levels taken by 3 smartphones

Figure 9(a) shows the relationships between albumin concentration levels and the intensity values of the original images, while Figure 9(b) shows the relationships between albumin concentration levels and the intensity values of

Algorithm 2: $BInGamma(img\_cal) : img\_big$

Require: img_cal: vector of calibrated urinalysis images
Ensure: img_big: vector of images after blind inverse gamma correction

$range \leftarrow [0.5 : 0.1 : 2.2]$
for $(\forall I_i \in img\_cal)$ **do**
  $I_i^{HSL} \leftarrow RGBtoHSL(I_i^{RGB})$
  $I_i^{L} \leftarrow Normalise(I_i^{L})$ {rescale L band to [0,1]}
  for $(\forall S_j \in I_i)$ **do**
    for $(\forall \gamma \in range)$ **do**
      $bic \leftarrow bispec(S_j^{1/\gamma})$ {Calculate bicoherence}
    end for
    $B(\gamma) \leftarrow mean(bic)$
  end for
  for $(\forall k \in vector(B))$ **do**
    $ind \leftarrow min(B(k))$
    $\gamma_{est} \leftarrow range(ind)$ {Calculate estimated gamma based on the rank of min(B)}
  end for
  $\overline{\gamma_{est}} \leftarrow mean(\gamma_{est})$
  $I_i^{L} \leftarrow (I_i^{L})^{1/\overline{\gamma_{est}}}$ {Apply $\overline{\gamma_{est}}$ as an inverse gamma to I_i^{L}}
  $I_i^{RGB} \leftarrow HSLtoRGB(I_i^{HSL})$
  $img\_big[i] \leftarrow I_i^{RGB}$
end for

return img_big

the colour-calibrated images. All the curve fittings in Figure 9 reveal a power correlation. While the curves for the original images show considerable discrepancy, those for the colour-calibrated images display reasonably consistent results as listed in Table 1, where N4's curve is slightly better than the other two and subsequently chosen to proceed with blind inverse gamma correction. The results have confirmed that the colour calibration process is able to tackle the diversity of smartphone cameras.

Table 1: Curve fittings for the 3 smartphones

Phone	MSE	Variance	St. Dev.	$R^2(y = ax^b)$
iPhone 6s	0.0006	0.0180	0.1252	0.9877
Galaxy N4	0.0009	0.0161	0.1133	0.9914
Galaxy S3	0.0000	0.0212	0.1233	0.9821

After performing blind inverse gamma correction on the calibrated images from N4, Figure 10(a) shows how image intensity responds to albumin concentration, while Figure 10(b) further depicts a linear relationship between the albumin concentration levels and the intensity values of blind inverse gamma corrected images after performing Principle Component Analysis (PCA). To verify this linear relationship, we use K-fold cross validation to model the correlation, which again exhibits a linear relationship as shown in Figure 10(c). Figure 10(d) reveals that the regression models derived independently with the two different techniques are almost identical.

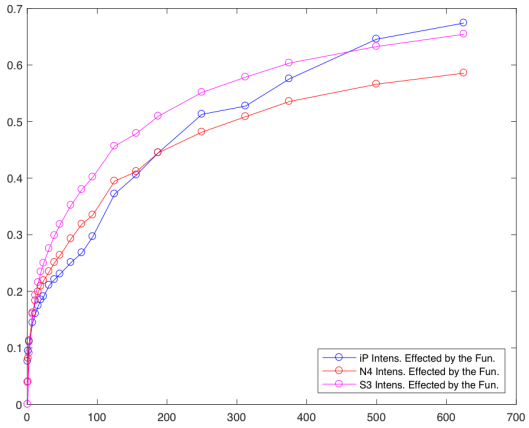

(a) Concentration vs. intensity of original images

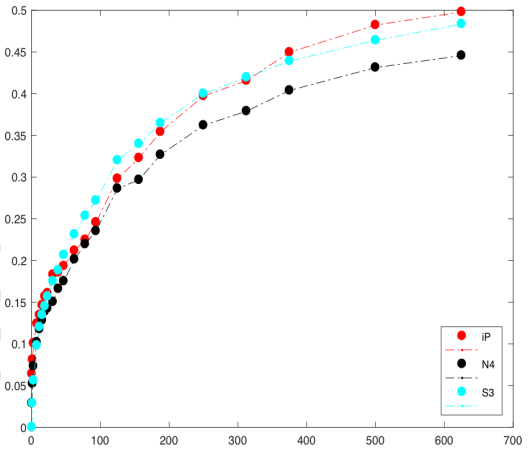

(b) Concentration vs. intensity of colour-calibrated images

Figure 9: Relationships between albumin concentration levels and the intensity values

No	Concentration (PCA)	Intensity (PCA)	Concentration (K-fold)	Intensity (K-fold)
1	1.953e+01	0.000627268	19.531	0.0006
2	2.34e+01	0.001134885	23.438	0.0011
3	3.13e+012	0.002149857	31.25	0.0022
4	3.91e+01	0.003164959	39.063	0.0032
5	9.38e+01	0.010270156	93.75	0.0103
6	156.25	0.018390455	156.25	0.0184
7	250	0.030570903	250	0.0306
8	375	0.046811501	375	0.0468
9	625	0.079292696	625	0.0793

Table 2: Random data predicted by PCA and K-fold models

Table 2 further lists some random data predicted by the two regression models. The results have confirmed that the blind inverse gamma correction process is able to tackle the non-linear correspondence between the image intensity values and the albumin concentration levels.

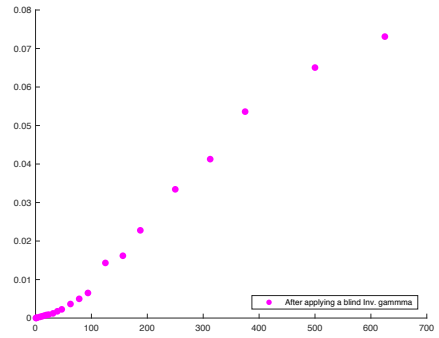

(a) Concentration vs. intensity of blind inverse gamma corrected images of N4

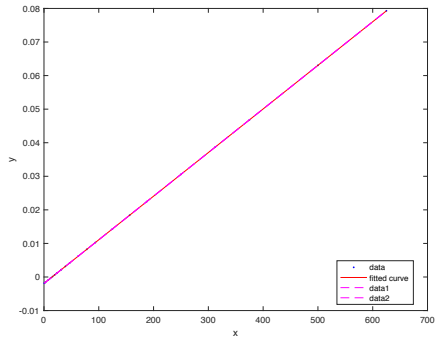

(b) Principle component analysis (PCA)

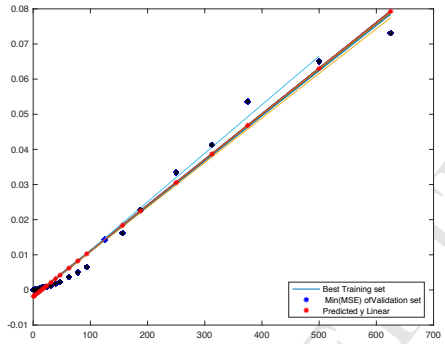

(c) K-fold cross-validation

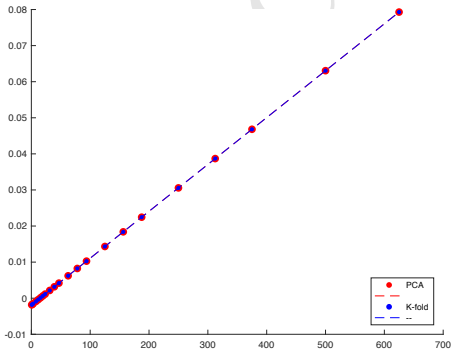

(d) PCA vs. K-fold

Figure 10: Relationship between albumin concentration levels and intensity values after blind inverse gamma correction

5. Urinalysis Mobile Application

A urinalysis mobile application is specially designed to complete the uTester device. Three design considerations were taken to address the device-agonistic issue: a) the application needs to be cross-platform including both Android and iOS, b) the application has a low requirement for smartphone hardware including CPU, GPU, RAM, and storage, and c) the application adopts a minimal user interface design so that it does not require too much screen real estate and is easy to use by elderly users.

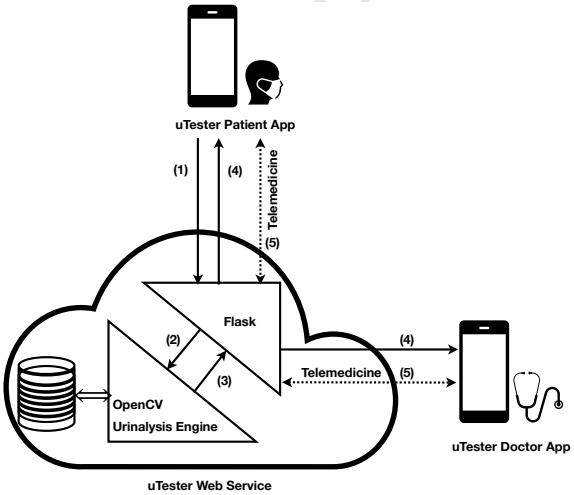

Figure 11: Architecture of the uTester mobile application

The final design is a hybrid thin mobile client - uTester Patient App - that is connected to a uTester Web Service provisioned by a cloud through Infrastructure as a Service (IaaS). The Patient App has two main functions of urinalysis and telemedicine. Figure 11 illustrates the architecture and workflow of the mobile application.

1. The uTester Patient App captures the test images and sends them to the Web Service.
2. The uTester Web Service receives the images, checks their validity, stores them into the database, and invokes OpenCV (Open Source Computer Vision Library) [63] to process and analyse the images (as discussed in Section 4) before passing on the retrieved image intensity values to the Urinalysis Engine. The Web Serice is provided by Flask [64], a micro web framework built in Python for fast development of scalable web applications. OpenCV is a library of programming functions aimed at real-time computer vision.
3. The Urinalysis Engine uses the prediction model to derive the albumin level in urine and passes the result on to Flask. Figure 12 shows a linear prediction model ($R^2 = 0.9856$, $SSE = 0.0001578$, and $RMSE = 0.002809$) with internals:

$$x = \frac{y-a}{b},$$

where y is the image intensity value, x is the predicted albumin level in urine, and $a = 0.0001299 \in [0.0001226, 0.0001372]$ and $b = -0.00191 \in$ [-0.003502, -0.000319] are the co-efficients (with 95% confidence bounds) derived from the training data.

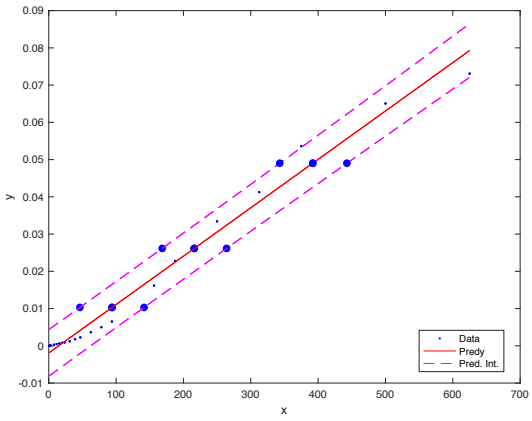

Figure 12: Linear prediction model with internals

4. Flask sends the test result in JSON (JavaScript Object Notation) format back to the Patient App, which displays (as shown in Figure 13(a)) it to the patient conducting the test. The result is also sent to the patient's doctor.
5. The doctor uses the uTester Doctor App to perform various telemedicine activities [65], for instance, electronic consultation [66] where the Doctor App interacts with the Patient App via the uTester Web Service.

This design has a number of advantages. First, the native mobile client is simple, easy to develop, and does not require much hardware resource. Second, the urinalysis application is adaptable to changes as new image processing and analysis techniques and more accurate urinalysis prediction models can be adopted without the need to update the native mobile client. Third, the urinalysis application is scalable with the growing number of images and test results. Last, the urinalysis application is resilient to the loss or replacement of smartphone as all the test images and results are securely stored in the cloud. An alternative design would be a fat native mobile application into which all the processing is built and all the data is stored, making it extremely heavyweight, inflexible and vulnerable to device agnosticism.

Alternative to a thin native mobile client is a pure web client, which is naturally cross-platform, however this is not a viable approach as a web client cannot access a smartphone's camera. Therefore, the mobile client is implemented separately for Android and iOS devices; nevertheless, Xamarin platform [67] has been used to develop the native mobile clients in order to allow for maximum code sharing. The Doctor App can be implemented as a pure web client if it does not need to access the smartphone's built-in sensors or peripheral devices. In contrast, if electronic consultation requires audiovisual communication between the doctor and the patient, it would have to be implemented as a native mobile client. However, the Doctor App is beyond the scope of this paper.

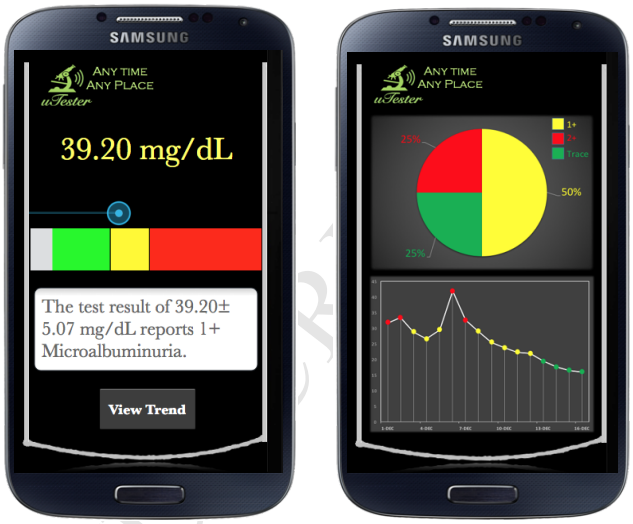

(a) Displaying the result **(b)** Viewing the trend

Figure 13: The minimal user interface of the uTester native mobile client

Figure 13(a) shows the minimal user interface of the mobile client displaying the current urinalysis result. It uses the traffic light metaphor to visualise the result: red denotes 2+ microalbuminuria (>100 mg/dL), yellow denotes 1+ microalbuminuria (30-100 mg/dL), green denotes trace (<30 mg/dL), and grey denotes no trace, followed by the explanation notes elaborating the current test result. All test images and results are timestamped and stored in the cloud so that the patient can view their urinalysis trend as shown in Figure 13(b). Table 3 (referring to Figure 12) shows 3 examples of smartphone-based urinalysis. In particular, for the image intensity of 0.049021, its alumin concentration is 39.20 ± 5.07 mg/dL, which corresponds to 1+ microalbuminuria, as shown in Figure 13(a).

Table 3: Examples of smartphone-based urinalysis

Image Intensity	Albumin Level (mg/dL)	Lower Bound	Upper Bound	Microalbuminuria Grading
0.010303	9.3998	4.6206	14.1511	Trace
0.026154	21.5999	16.8449	26.4094	Trace
0.049021	39.2001	34.2989	44.2745	1+

6. Conclusions and Future Work

This paper has presented the design and development of a smartphone-based urinalysis device that has the ability for CKD patients themselves to conduct rapid and reliable quantitative diagnosis of albumin in urine, focusing on addressing the device agnosticism issue. The proposed solution comprises a custom-designed imaging housing that can be attached to smartphones of varying dimensions and

camera positions, an imaging processing and analysis process that can retrieve accurate properties (comparable to those used by the training dataset) of images captured by different smartphones, and a specially designed cross-platform urinalysis mobile application. Preliminary evaluation of the device has confirmed the effectiveness of the proposed solution to device agnosticism and the viability of a smartphone-based device for POC quantitative urinalysis.

We are conscious of the limitations of the current uTester prototype and the underpinning techniques. There is still a long way to go before the device is ready to be used by patients. First is regarding the BSPOTPE bioprobe, which can be used to test up to 1+ microalbuminuria. Work is ongoing to synthesise an optimal BSPOTPE that can measure up to 4+ microalbuminuria. Furthermore, as the albumin concentration in a urine sample is affected by hydration, it has become customary to measure albumin-to-creatinine ratio (ACR) as creatinine excretion is considered to be fairly constant throughout the day [16]. Therefore, we are also in the process of synthesising AIE-based creatinine bioprobe.

Second is regarding the imaging housing. More work is required to make it more affordable, portable, and usable to older people, the main source of CKD patients. Prior cognitive psychology research into user centred design, investigating product and interface usability, have all found that prior experience is the leading contributor to intuitive use. Therefore device fabrication and usability should be designed in such a way that its use is familiar and where the learning of new and unfamiliar tasks can be minimised [68, 50]. The last is regarding a systematic evaluation of the device, including testing with more brands of smartphones, verifying the device's test accuracy first through controlled artificial urine samples and then through real urine samples by comparing its test results against laboratory test results [38]. The evaluation also includes usability study of the device such as the ergonomics of the device, the usability of the mobile application interface, and the human factors involved in using the device, including physical, physiological, psychological, emotional, and cognitive factors.

Acknowledgements

The authors wish to thank Matthew Keen, Nathan West, and Ravichandran Rasiah for their contributions to the project. The authors are also grateful for the constructive suggestions made by the reviewers to improve the paper.

References

[1] W. Couser, G. Remuzzi, S. Mendis, M. Tonelli, The contribution of chronic kidney disease to the global burden of major noncommunicable diseases, Kidney Int 80 (2011) 1258–1270.

[2] S. White, K. Polkinghorne, R. Atkins, S. Chadban, Comparison of the prevalence and mortality risk of CKD in Australia using the CKD Epidemiology Collaboration (CKD-EPI) and Modification of Diet in Renal Disease (MDRD) Study GFR estimating equations: the AusDiab (Australian Diabetes, Obesity and Lifestyle) Study, American Journal of Kidney Diseases 55 (4) (2010) 660–70.

[3] D. Johnson, Evidence-based guide to slowing the progression of early renal insufficiency, Intern Med J 34 (2004) 50–57.

[4] K. Iseki, Ykemiya, C. Iseki, S. Takishita, Proteinuria and the risk of developing end-stage renal disease, Kidney Int 63 (2003) 1468–1474.

[5] W. Hoy, Z. Wang, P. V. Buynder, P. Baker, S. McDonald, J. Mathews, The natural history of renal disease in australian aborigines. part 2. albuminuria predicts natural death and renal failure, Kidney Int 60 (2001) 249–256.

[6] J. A. Beto, K. A. Schury, V. K. Bansal, Strategies to promote adherence to nutritional advice in patients with chronic kidney disease: a narrative review and commentary, International Journal of Nephrology and Rsnovascular Disease 9 (2016) 21–33.

[7] W. Keane, G. Eknoyan, Proteinuria, albuminuria, risk, assessment, detection, elimination (parade): a position paper of the national kidney foundation, Am J Kidney Dis 33 (5) (1999) 1004–10.

[8] P. H. Winocour, Microalbuminuria, BMJ 304 (6836) (1992) 1196–1197.

[9] D. W. Johnson, G. R. D. Jones, T. H. Mathew, M. J. Ludlow, S. J. Chadban, T. Usherwood, K. Polkinghorne, S. Colagiuri, G. Jerums, R. MacIsaac, H. Martin, Chronic kidney disease and measurement of albuminuria or proteinuria: a position statement, The Medical Journal of Australia 197 (4) (2012) 224–225.

[10] P. Ruggenenti, F. Gaspari, A. Perna, G. Remuzzi, Cross sectional longitudinal study of spot morning urine protein:creatinine ratio, 24 hour urine protein excretion rate, glomerular filtration rate, and end stage renal failure in chronic renal disease in patients without diabetes, BMJ 316 (7130) (1998) 504–9.

[11] A. F. Coskun, R. Nagi, K. Sadeghi, S. Phillips, A. Ozcan, Albumin testing in urine using a smart-phone, Lab on a Chip 13 (2013) 4231–4238.

[12] W. Laiwattanapaisal, T. Songjaroen, T. Maturos, T. Lomas, A. Sappat, A. Tuantranont, On-chip immunoassay for determination of urinary albumin, Sensors 9 (12) (2009) 10066–10079.

[13] D. Wong, S. Giguère, M. Wendel, Evaluation of a point-of-care portable analyzer for measurement of plasma immunoglobulin g, total protein, and albumin concentrations in ill neonatal foals, J Am Vet Med Assoc. 242 (6) (2013) 812–9.

[14] H. L. Heerspink, E. Witte, S. Bakker, P. de Jong, D. de Zeeuw, R. Gansevoort, Screening and monitoring for albuminuria: the performance of the hemocue point-of-care system, Kidney Int 74 (3) (2008) 377–383.

[15] S. White, R. Yu, J. Craig, K. Polkinghorne, R. Atkins, S. Chadban, Diagnostic accuracy of urine dipsticks for detection of albuminuria in the general community, Am J Kidney Dis (58) (2011) 19–28.

[16] KDIGO, Kdigo 2012 clinical practice guideline for the evaluation and management of chronic kidney disease, Kidney International Supplements 3 (1) (2013) 19–62.

[17] Diagnostic Evidence Co-operative Oxford, Point-of-care creatinine testing for the detection and monitoring of chronic kidney disease, Tech. Rep. Horizon Scan Report 0038, National Institute for Health Research (2014).

[18] DCA Vantage: Analyzer Drive diabetic patient compliance with trusted, clinically proven results [cited 23/11/2017].
URL `http://www.healthcare.siemens.com.au/point-of-care/diabetes/dca-vantage-analyzer`

[19] E. Agu, P. Pedersen, D. Strong, B. Tulu, Q. He, L. Wang, Y. Li, The smartphone as a medical device: Assessing enablers, benefits and challenges, in: Proceedings of IEEE International Conference on Sensing, Communications and Networking, 2013, pp.

76–80.

[20] J. Alexander, G. Joshi, Smartphone application-based medical devices: twenty-first century data democratization or anarchy?, International Anesthesia Research Society 123 (4) (2016) 1046–50.

[21] B.-Y. Chang, Smartphone-based chemistry instrumentation: Digitization of colorimetric measurements, Bulletin of the Korean Chemical Society 33 (2) (2012) 549–552.

[22] D. Erickson, D. O'Dell, L. Jiang, V. Oncescu, A. Gumus, S. Lee, M. Mancuso, S. Mehta, Smartphone technology can be transformative to the deployment of lab-on-chip diagnostics, Lab on a Chip 14 (17) (2014) 3159–64.

[23] A. Landman, S. Emani, N. Carlile, D. Rosenthal, S. Semakov, D. Pallin, E. Poon, A mobile app for securely capturing and transferring clinical images to the electronic health record: Description and preliminary usability study, JMIR Mhealth Uhealth 3 (1) (2015) 3481.

[24] J. Oresko, Z. J. andJun Cheng, S. Huang, Y. Sun, H. Duschl, A. Cheng, A wearable smartphone-based platform for real-time cardiovascular disease detection via electrocardiogram processing, IEEE Transactions on Information Technology in Biomedicine 14 (3) (2010) 734 – 740.

[25] V. Oncescu, M. Mancuso, D. Erickson, Cholesterol testing on a smartphone, Lab on a Chip 14 (2014) 759–763.

[26] J. Tran, R. Tran, J. R. W. Jr., Smartphone-based glucose monitors and applications in the management of diabetes: An overview of 10 salient "apps" and a novel smartphone-connected blood glucose monitor, Clinical Diabetes 30 (4) (2012) 173–178.

[27] S. D. Kim, Y. Koo, Y. Yun, A smartphone-based automatic measurement method for colorimetric ph detection using a color adaptation algorithm, Sensors 17 (7) (2017) 1604.

[28] S. Kroemer, J. Frühauf, T. Campbell, C. Massone, G. Schwantzer, H. Soyer, R. Hofmann-Wellenhof, Mobile teledermatology for skin tumour screening: diagnostic accuracy of clinical and dermoscopic image tele-evaluation using cellular phones, British Journal of Dermatology 164 (5) (2011) 973–9.

[29] S. Razdan, J. Johannes, R. Kuo, D. Bagley, The camera phone: a novel aid in urologic practice, Urology 67 (4) (2006) 665–9.

[30] M. Yamada, H. Watarai, T. Andou, N. Sakai, Emergency image transfer system through a mobile telephone in japan: technical note, Neurosurgery 52 (4) (2003) 986–90.

[31] A. Skandarajah, C. D. Reber, N. A. Switz, D. A. Fletcher, Quantitative imaging with a mobile phone microscope, PloS one 9 (5) (2014) e96906.

[32] M. Bigas, E. Cabruja, J. Forest, J. Salvi, Review of cmos image sensors, Microelectronics Journal 37 (5) (2006) 433–51.

[33] A. K. Yetisena, J. Martinez-Hurtadoa, A. Garcia-Melendrez, F. da Cruz Vasconcellos, C. R. Lowe, A smartphone algorithm with inter-phone repeatability for the analysis of colorimetric tests, Sensors and Actuators B: Chemical 196 (2014) 56–160.

[34] D.-S. Lee, B. G. Jeon, C. Ihm, J.-K. Park, M. Y. Jung, A simple and smart telemedicine device for developing regions: a pocket-sized colorimetric reader, Lab on a Chip 11 (2011) 120–126.

[35] L. Shen, J. A. Hagen, I. Papautsky, Point-of-care colorimetric detection with a smartphone, Lab on a Chip 12 (2012) 4240–4243.

[36] J. I. Hong, B.-Y. Chang, Development of the smartphone-based colorimetry for multi-analyte sensing arrays, Lab on a Chip 14 (2014) 1725–1732.

[37] M. Ra, M. S. Muhammad, C. Lim, S. Han, C. Jung, W.-Y. Kim, Smartphone-based point-of-care urinalysis under variable illumination, IEEE Journal of Translational Engineering in Health and Medicine 6 (2018) 2800111.

[38] K. Choi, I. Chang, J. Lee, d. K. Kim, S. Noh, H. Ahn, J. Cho, Y. Kwak, S. Kim, H. Kim, Smartphone-based urine reagent strip test in the emergency department, Telemedicine and e-Health 22 (6) (2016) 10.1089/tmj.2015.0153.

[39] H Tong and Y Hong and Y Dong and M Häussler and Z Li and JW Lam and Y Dong and HH Sung and ID Williams and BZ Tang, Protein detection and quantitation by tetraphenylethene-based fluorescent probes with aggregation-induced emission characteristics, The Journal of Physical Chemistry 111 (40) (2007) 1817–11823.

[40] M. Kessler, A. Meinitzer, W. Petek, O. Wolfbeis, Microalbuminuria and borderline-increased albumin excretion determined with a centrifugal analyzer and the albumin blue 580 fluorescence assay, Clinical Chemistry 43 (6) (1997) 996–1002.

[41] S. Akraa, F. Guo, H. Shen, Y. Tang, J. Li, G. Lee, B. Tang, On the feasibility of a smartphone-based solution to rapid antitative urinalysis using nanomaterial bioprobes, in: Proceedings of the 14th International Conference on Mobile and Ubiquitous Systems: Computing, Networking and Services (MobiQuitous), 2017.

[42] J. Mei, Y. Hong, J. W. Y. Lam, A. Qin, Y. Tang, B. Z. Tang, Aggregation-induced emission: The whole is more brilliant than the parts, Advanced Materials 26 (31) (2014) 5429–5479.

[43] S. Chutipongtanate, V. Thongboonkerd, Systematic comparisons of artificial urine formulas for in vitro cellular study, Anal Biochem 402 (1) (2010) 110–112.

[44] Cold Spring Harbor Protocols [cited 23/11/2017]. [link].
URL `http://cshprotocols.cshlp.org/content/2006/1/pdb.rec8247.full?text_only=true`

[45] Proteinuria [cited 23/11/2017].
URL `https://en.wikipedia.org/wiki/Proteinuria`

[46] Y. Hong, C. Feng, Y. Yu, J. Liu, J. W. Y. Lam, K. Q. Luo, B. Z. Tang, Quantitation, visualization, and monitoring of conformational transitions of human serum albumin by a tetraphenylethene derivative with aggregation-induced emission characteristics, Analytical Chemistry 82 (2010) 7035–7043.

[47] T. Chen, N. Xie, L. Viglianti, Y. Zhou, H. Tan, B. Z. Tang, Y. Tang, Quantitative urinalysis using aggregation-induced emission bioprobes for monitoring chronic kidney disease, Faraday Discussions 196 (2016) 351–362.

[48] T. B. Moeslund, Introduction to Video and Image Processing: Building Real Systems and Applications, Springer, 2012.

[49] A. Blackler, V. Popovic, Towards intuitive interaction theory, Interacting with Computers 27 (3) (2015) 203–209.

[50] M. A. O'Brien, W. A. Rogers, A. D. Fisk, Developing a framework for intuitive human-computer interaction, in: Proceedings of 52nd Annual Meeting of the Human Factors and Ergonomics Society., Vol. 52, 2008, pp. 1645–1649.

[51] H. Nour Abura'ed, F. Khan, High-iso image de-noising using burst filte, in: Proceedings of IEEE 59th International Midwest Symposium on Circuits and Systems, 2016, pp. 1–4.

[52] S.-C. Tai, T.-W. Liao, Y.-Y. Chang, C.-P. Yeh, Automatic white balance algorithm through the average equalization and threshold, in: Proceedings of 8th IEEE International Conference on Information Science and Digital Content Technology, 2012, pp. 571–576.

[53] B. Zhang, A. Batur, A real-time auto white balance algorithm for mobile phone cameras, in: Proceedings of IEEE International Conference on Consumer Electronics, 2012, pp. 1–4.

[54] F. Xiao, J. E. Farrell, J. M. DiCarlo, B. A. Wandell, Preferred color spaces for white balancing, in: Proc. SPIE 5017, Sensors and Camera Systems for Scientific, Industrial, and Digital Photography Applications IV, 2003.

[55] P. Au, M. Donn, Hdr luminance measurement: Comparing real and simulated data, in: Proceedings of 46th ANZAScA Conference of the Architectural Science Association, 2003.

[56] A. Ford, A. Roberts, Colour space conversions, Westminster University, London, 1998.

[57] R. Jayashree, RGB to HSI color space conversion via MACT algorithm, in: International Conference on Communications and Signal Processing (ICCSP), 2013, pp. 561–565.

[58] I. Sanza, L. Muserosa, Z. Falomirb, L. Gonzalez-Abrilc, Customising a qualitative colour description for adaptability and usability, Pattern Recognition Letters 67 (1) (2015) 2–10.

[59] M. Anthimopoulos, S. Gupta, S. Arampatzis, S. Mougiakakou, Smartphone-based urine strip analysis, in: Proceedings of IEEE International Conference on Imaging Systems and Techniques, 2016.

[60] A. Ilie, G. Welch, Ensuring color consistency across multiple

cameras, in: Proceedings of 10th IEEE International Conference on Computer Vision (ICCV), 2005.
[61] Y. Cao, X. Pan, X. Zhao, H. Wu, An analog gamma correction scheme for high dynamic range cmos logarithmic image sensors, Sensors 14 (12) (2014) 24132–45.
[62] H. Farid, Blind inverse gamma correction, IEEE Transactions on Image Processing 10 (10) (2001) 1428–1433.
[63] G. Bradski, A. Kaehler, Learning OpenCV 3, Computer Vision in C++ with the OpenCV Library, O'Reilly Media, 2016.
[64] Welcome — Flask (A Python Microframework) [cited 23/11/2017].
URL `http://flask.pocoo.org`
[65] Telemedicine [cited 23/11/2017].
URL `https://en.wikipedia.org/wiki/Telemedicine`
[66] J. Stoves, J. Connolly, C. K. Cheung, A. Grange, P. Rhodes, D. O'Donoghue, J. Wright, Electronic consultation as an alternative to hospital referral for patients with chronic kidney disease: a novel application for networked electronic health records to improve the accessibility and efficiency of healthcare, Qual Saf Health Care 19 (2010) e54.
[67] Xamarin: deliver native Android, iOS, and Windows apps, using existing skills, teams, and code [cited 23/11/2017].
URL `https://www.xamarin.com/platform`
[68] A. Blackler, V. Popovic, D. Mahar, Investigating users' intuitive interaction with complex artefacts, Applied Ergonomics 41 (1) (2010) 72–92.